

GEOMETRICAL NONLINEARITY OF HIGH ASPECT RATIO WING AND VALIDATION VIA VIDEOGRAMMETRIC MEASUREMENT TECHNIQUE

Norzaima Nordin^{a*}, Baizura Bohari^a, Muhammad Badruzaman Jemat^b, Mohammad Yazdi Harmin^c

^a Department of Aeronautical Engineering and Aviation, Faculty of Engineering, National Defence University of Malaysia, Sungai Besi Camp, 57000 Kuala Lumpur, Malaysia

^b Department of Mechanical Engineering, Faculty of Engineering, National Defence University of Malaysia, Sungai Besi Camp, 57000 Kuala Lumpur, Malaysia

^c Department of Aerospace Engineering, Faculty of Engineering, Universiti Putra Malaysia 43400 Serdang, Selangor, Malaysia

ARTICLE INFO

ARTICLE HISTORY

Received: 15-06-2023

Revised: 01-09-2023

Accepted: 31-10-2023

Published: 31-12-2023

KEYWORDS

High aspect ratio

Geometrical nonlinearity

Ground static test

Videogrammetric measurement technique

ABSTRACT

The high aspect ratio (HAR) wing aircraft design has significant advantages due to its high lift characteristics with less-induced drag. However, its high flexibility leads to larger deformation and inexplicit geometrical nonlinear response. The nonlinear effects must be prudently determined to predict the behaviour of HAR wing. Despite the development of nonlinear geometrical model, HAR wing has been infrequently validated. Previous experimental studies mostly focused on the contact method and this technique is not reliable to HAR wing since it will alter the mass and stiffness of the structure. Addressing that, this study proposed a non-contact method using videogrammetric measurement technique to examine the geometrical nonlinearity effects. Ultrahigh-speed camera was used for motion capture and a novel approach using z-indicator was proposed to measure wing deformation. All experimental data were validated through the conventional finite element. A larger wing deflection were found proportionate with the longer wingspan. The high percentage difference between linear and nonlinear static analyses reaffirmed the significant need to consider geometrical nonlinear effects. Moreover, the comparison data recorded (low) percentage error of less than 10% for each aspect ratio. With that, the current study successfully developed an applicable novel technique for the measurement of HAR wing deflection.

1.0 INTRODUCTION

The drive to maximise and enhance operational and environmental efficiency has propelled the constant transformation and development of aircraft. Moreover, the rapid growth of the aviation industry comes with environmental concerns [1-2]. Addressing the economic and environmental demands for the continuous growth of the aviation industry, the government and other key stakeholders of the aviation industry, including aircraft manufacturing ensure the implementation of appropriate reduction of noise pollution, pollutant emission and carbon dioxide (CO₂) emission. The proportional relationship between fuel use in an aircraft engine and carbon emission from the aircraft depends on the types of aircraft, engine and fuel used, as well as the engine load and flying altitude [3]. The carbon emission of commercial aviation is about 2% to 3% and with the current growth rate, its contribution to the global carbon emission may increase up to 15% by 2050 [4]. Therefore, the International Air Transport Association (IATA) designed a CO₂ emission reduction roadmap to develop green aircraft technology, which involves the commitment of all key stakeholders of the aviation industry to reduce carbon emissions by 2050 [5]. One of the pivotal pieces of information in aircraft marketing involves the emphasis on the range and endurance characteristics in order to optimise the aircraft design according to the needs or requirements of a specific mission. This can be idealised through three approaches of the Breguet range equation:

*Corresponding Author | Nordin, N. | norzaima@upnm.edu.my

$$\text{Range} = \frac{L}{D} \frac{V}{TSFC} \ln \left(\frac{W_i}{W_f} \right) \quad (1)$$

where L , D , V , $TSFC$, W_i and W_f are the lift, drag, velocity, thrust specific fuel consumption, initial and final weight, respectively.

Based on Equation (1), the following alterations potentially influence the performance range of an aircraft: (1) through the improvement of engine performance ($V/TSFC$); (2) through the reduction of structural weight, resulting in the increase of (W_i/W_f) term; (3) through the improvement of aerodynamic performance that involves increasing the lift-to-drag ratio (L/D) via the increase of the aspect ratio of the wing. The purpose of the aircraft design (either for long endurance or high manoeuvrability) influences the selection of the above alterations. The development of an aircraft that can endure long operation with low fuel consumption typically requires the high aspect ratio (HAR) wing design, which offers the necessary stability and involves low fuel consumption and less-induced drag [6-7]. However, the manoeuvrability of such aircraft would be compromised. Despite the significance of HAR wing design, its application still requires improvement and optimisation due to its structural design that creates a geometrical nonlinear issue. The limited understanding on the aeroelastic behaviour of HAR wing design has led to the underdevelopment of its design. Under the same flight condition and aerodynamic load, a HAR wing would encounter a larger deformation issue due to its flexibility problem [8]. The changes in the dynamic behaviour and aeroelastic response of the wing design unfavourably lead to nonlinear instability [9]. One prominent example that describes the aeroelastic problem of a HAR wing is the failure of the NASA Helios prototype with the aspect ratio of AR-30.9, which led to its crash in the Pacific Ocean [10]. The use of linear analysis without considering the nonlinearity response leads to inaccurate modelling of the aeroelastic response of the wing. The wing structure cannot maintain its constant stiffness when large deformation occurs [11]. Consequently, the wing structure cannot return to its original structure even when the load is lifted. At this point, a nonlinear analysis is clearly necessary. The failure of the Helios prototype signifies the importance of understanding how the nonlinearity approach influences the aeroelastic behaviour of the HAR wing to approach the real behaviour of the high deflection wing. This scenario also reaffirms the invalidity of the conventional linear approach. When it comes to the analysis of the HAR wing structure, it is imperative to consider the nonlinearity effects.

Various techniques have been used to measure the geometrical nonlinearity (wing deformation), either using a contact or non-contact method. For instance, in the contact method, Lokos et al., [12] performed a ground load test to characterise the wing behaviour and quantify the torsional stiffness of the F/A-18 airplane at the NASA Dryden Flight Research Centre. The study added constraint at the main landing gear of the airplane and placed 48 markings on the left wing. Digital dial gauges and string potentiometers were attached along the aft, front, intermediate and rear spars to measure the deformation of the wing. In a similar study, Lizotte and Lokos [13] used an additional deflection-based load estimation (DBLE) technique. In particular, the study conducted the load calibration test by placing string potentiometers at 16 points of the F/A-18 upper surface left wing. Likewise, Northington and Pasilliao [14] placed string potentiometers along the spanwise of F-16 aircraft and found a good consistent correlation with the static analysis of conventional FE. Gharibi et al., [15] similarly applied the ground load tests and validated the results of wing deflection with simulation data. The study considered a total of eight loading points with appropriate displacement indicators over each point. The results of wing deflection were found to be in line with the outcomes of the simulation and experimental study. However, comparative studies on geometrical nonlinearity techniques using the contact method have remained scarce, particularly towards the HAR wing application, since this approach will modify the mass and stiffness of flexible wing structures.

The videogrammetric model deformation (VMD) measurement technique is one of the widely known techniques of a non-contact method. As it is a non-contact method and does not alter the mass or wing model stiffness, this measurement technique is deemed fitting for flexible wing structures. This technique depends on the optical method of measuring aeroelastic deformation in the wind tunnel. It involves the application of a single-camera or a multiple-camera approach. For instance, Burner and Liu [16] proposed the use of a single-camera VMD system and set it up with a charge-coupled device (CCD) camera, a computer with image acquisition and a light source for the target placed on a wing model. For the calculation of the bending and twist deflections of the wing model, the study applied a linear fitting method (for twist calculation according to the local angle of attack that fits the target coordinate in x -plane and z -plane) and least-square method (for determination of wing bending deflection). Barrows [17]

incorporated the same technique with passive and active targeting using photogrammetry and projection moiré interferometry (PMI). The retro-reflective target (passive target) was placed on the wing element, which served as a baseline for the comparison of results between the condition of wind-off and wind-on in the wind tunnel test. Meanwhile, Pitcher et al., [18] applied the VMD technique to examine the wing motion of the flexible nighthawk mini-UAV.

The standard VMD technique was extended to the resonance shape and spectral analysis of the flapping behaviour of the wing model. A non-coded target in circular dots and a coded target surrounded by banded sections were subjected to the wind tunnel test. Accordingly, the process of calibrating the camera is pivotal in the videogrammetric measurement technique. The location of the principal point, the focal length (zoom) and de-centre camera lens distortion were calculated during the calibration process. Following that, the camera is positioned to capture the image sets with the identified targets. To capture high-quality images, it is necessary to have proper lighting that illuminates high-contrast targets without producing glare off the wing, the wind-tunnel viewing glass, or the wind-tunnel floor that may wash out the targets or cause false targets. The location of each target within each frame is then exported to a data file. Zhang et al., [19] applied the same approach to supersonic wind tunnel facilities. The study set up two cameras with 4,000,000 pixels and fixed focus lens for the videogrammetric system. However, prior studies mainly focused on the low aspect ratio (LAR) wing. For the single-camera approach, previous work did not clearly state the required measurement technique. Moreover, only a few studies reported the validation of the experimental data with the numerical model. Therefore, the current study primarily aimed to examine the influence of geometrical nonlinearity focusing on the HAR wing with the different aspect ratios. Furthermore, an ultrahigh-speed camera was used as a preliminary measurement tool to obtain accurate outcomes of the HAR wing deformation via videogrammetric measurement technique for a ground static test (GST) application. This novel technique of using the ultrahigh-speed camera was considered prior to its application in the wind tunnel test.

2.0 METHODOLOGY

This section describes the simulation and ground static test setup of the HAR wing model with the usage of an ultrahigh-speed camera. The idea behind this ground static test setup was also used to develop a videogrammetric measurement technique for HAR wing deformation prior to the wing tunnel test. At this stage, four variants of half wingspan aspect ratios of AR-10, AR-12, AR-14 and AR-16 were used to verify with the conventional finite element (FE) of nonlinear static analysis.

2.1 Finite Element Analysis (Simulation) Setup

Several steps were carried out in the finite element analysis setup starting with the pre-processing stage, which involved an input file containing structural data; geometry (wing structure model), meshing, material properties, boundary conditions, force applied and the type of solution. Focusing on the objectives to examine the effect of geometrical nonlinearity at different aspect ratios, both geometric linear and nonlinear analyses were performed using the FE solver of MSC Nastran 2017 with the respective solution control code (SOL 101 and SOL 106). In the processing stage, the input file (.DAT or .bdf format) was automatically sent to the solver and the output file (.f06) will then be post-processed using MATLAB programming for result analysis (in terms of wing displacement). The aspect ratio of AR-10 was served as the minimum baseline and the aspect ratio of AR-16 was set as the maximum baseline. The aspect ratio of the HAR wing model was altered by extending the span length with a constant chord length value of 0.05 m. For the modification of aspect ratios, the span length was extended with a constant chord length. The details of meshing, material properties, boundary condition entry for spars, fairings and ribs in this study were adopted from Nordin et al., [20] and provided in Table 1. The analysis began with a parametric study that examined the deviation in vertical tip displacement at different aspect ratios between linear and nonlinear static analyses. The analysis also served to validate the data of nonlinear static analysis with experimental data in the ground static test. Accordingly, the employed linear static analysis was based on the following assumptions: (1) the use of linear equation from the simplification of Hooke's law; (2) static analysis that is independent of time. Unlike the linear static analysis (an independent load condition represents the subcases for a case control), the initial condition for the subsequent subcase for nonlinear static analysis depends on the end condition of the prior subcase and the Newton-Raphson iterative method is applied to iteratively address the solution. The programme continuously updates the stiffness matrix at every iteration, starting from the initial input at 1% of the total load, until the convergence of the solution for all load steps is attained. The analysis continues to

reassemble and resolve the stiffness matrix with updated information if it fails to achieve the convergence of the solution at the first place. Only after the convergence is attained, the displacement results are obtained.

Table 1. Geometric and material properties of HAR wing components [20]

Geometric Properties		AR-10	AR-12	AR-14	AR-16
Half wingspan length, L_s		0.5 m	0.6 m	0.7 m	0.8 m
Wing chord length, L_c		0.05 m	0.05 m	0.05 m	0.05 m
Wing Component	Material	Properties		Value	
Spar	Spring steel	Young modulus, E_s		207 GPa	
		Density, ρ_s		7833.41 kgm ⁻³	
		Poisson's ratio, ν_s		0.295	
Fairings	Styrofoam	Density, ρ_f		127.6 kgm ⁻³	
Ribs	ABS	Density, ρ_r		1264.83 kgm ⁻³	

3.0 EXPERIMENTAL SETUP

This study mainly aimed to develop a robust and accurate videogrammetric measurement technique for HAR wing deformation using the ultrahigh-speed camera prior to the wind tunnel test. Four specified aspect ratios of AR-10, AR-12, AR-14 and AR-16 were used sequentially to validate the recorded wing deformation results with the results of the designated nonlinear static analysis in simulation. For this study, the HAR wing model, which included spars, fairings and ribs, replicated the HAR wing simulation model. The spar section of a flat plate with constant width (0.025 m) and thickness (0.00125 m) was fabricated from a spring steel sheet with different lengths (0.5 m, 0.6 m, 0.7 m and 0.8 m).

The Phantom V1211 digital ultrahigh-speed camera has been used throughout this experimental work with the ability to capture up to 12 gigapixels per second (Gpx/s) data with a high resolution of the complementary metal oxide semiconductor (CMOS) sensor. The camera can capture 12,000 frames per second (fps) at a full resolution of 1280 × 800 pixels. A user-friendly phantom camera control (PCC) software that comes with 2-D motion analysis tools was used to control this ultrahigh-speed camera. This software is capable to calculate the required measurements in terms of position, distance, angle, velocity, angular speed measurements, track multiple objects or points and generate graphs in xy -coordinates. The setup of videogrammetric measurement technique consists of the Phantom V1211 ultrahigh-speed camera with Nikon lens, ethernet LAN cable, DC input cable and host computer. The camera is positioned facing the wing model mounted at the load application structure as depicted in Figure 1. The distance of the camera and the wing was adjusted until a good visual was obtained in the PCC software. There are a few requirements at the initial stage of the pre-installation check. The main important part is the IP address setting of the phantom control unit (PCU). In this study, the IP address will be set as per Phantom V1211 manual reference (100.100.100.1) with a sub-network set to (255.255.0.0) [21].

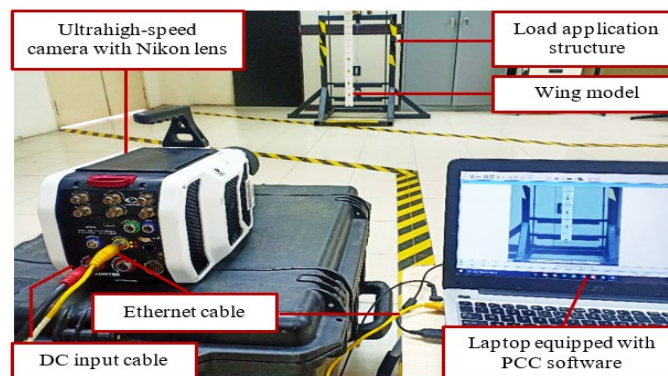


Figure 1. Setup of the ultrahigh-speed camera for the ground static test

For this calibration process, a measurement scale of a specified number of pixels to a unit scale size (in meter) was determined. The measurement scale was defined based on two selected points on the PCC image with a known scale (in meter). For instance, the resolution used in the ground static test is 768 pixels, with actual captured distance is 0.4 m; this implies that each pixel produces about 0.00052

m/pixel. This step was deemed essential to ensure no wrong track of any pixel that may contribute measurement error. The current study's pre-test revealed 0.389 m, with the original measurement of 0.4 m. As a result, the error was below 3%. For this wing model, the origin was established at the centre wingtip chord, which served as a reference measurement point for xy -direction. The third step involved using the PCC software to set the specification of the camera according to the environment before the motion of the wing was captured in a high-quality video. A relatively high number of fps and exposure time were required to capture the motion of the wing. The high interval of the PCC camera with 10,000 microseconds can capture and measure high-speed motion. The applied load at the static point was slowly released to prevent the interference of the load and rope with the selected tracking point. The motion of the wing (deflection) was recorded and saved for the measurement process as shown in Figure 2. This entire process was repeated three times for the applied load of 0.5 N until 3.5 N.

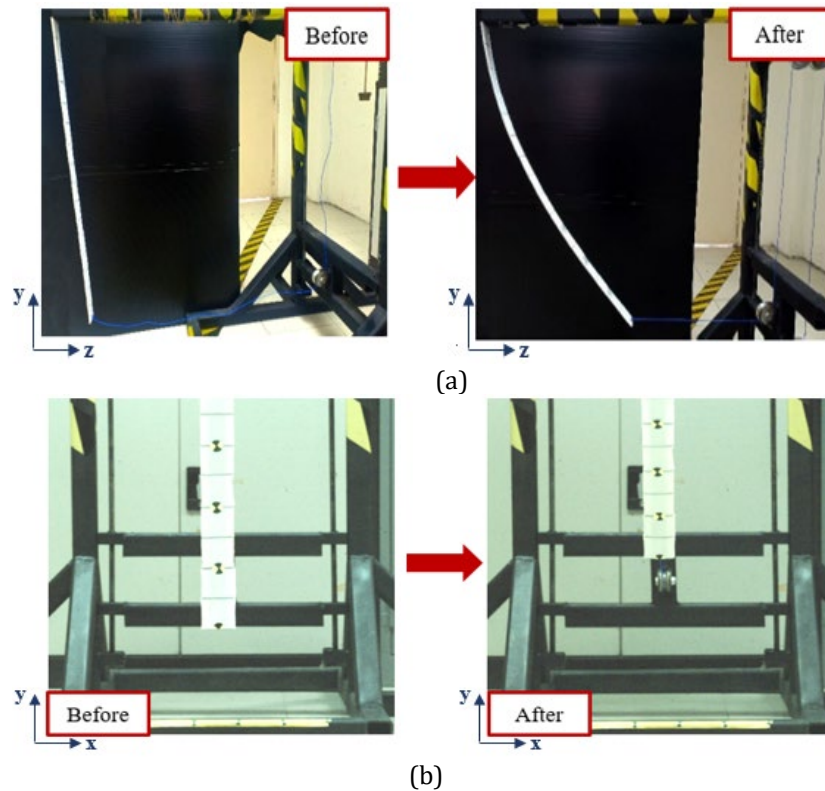


Figure 2. Snapshot of wing motion before and after load released (a) real image (b) PCC view

The PCC software is a 2-D motion analysis tool with xy -coordinate measurement. As for the current study's ground static test, only y -coordinate measurement was considered. The gathered data were interpolated with a z -indicator for the definition of tip deflection in the z -direction. In order to prevent the wing model from rotating in the x -direction, the wing root was clamped at the end of the mounting structure. For the ground static test, only the measurement at the wingtip was considered and validated with simulation data. For reproducibility, the selected tracking points must stand out against the background colour in the PCC image. The recording proceeded until full wing deflection (due to the applied loads) was achieved. The coordinate measurements were determined from the origin point pixel defined in the prior step. The coordinates of the moving points were saved in Microsoft PowerPoint (.pps) file format before the data were exported to Microsoft excel (.xlsx). Meanwhile, the subtraction of the y -coordinate after and before the deflection of the wing resulted in the displacement of the wing deflection at the wingtip in the y -direction. In this study, all experiments were repeated three times for accuracy and reproducibility. The average value of y -deflection data was recorded for each applied load. All recorded data were utilised and interpolated to determine the deflection of the HAR wing in the z -direction.

The deflection of the HAR wing in the z -direction was determined based on the identified z -indicator. This step represented the most important process of ensuring the correct reference for z -deflection value for the comparison between experimental and simulation data. The top mounting of the load application structure and the floor was equally marked 10 cm from the wing until 50 cm behind the path of the wing

deflection. The free end of the vertically attached ropes at each marking was then manually pulled until the desired distance for the wingtip was achieved as shown in Figure 3. The measurement process at this point applied the exact same procedure described in the prior subsection. The movement of the wing was recorded, and the PCC software was used for the measurement of y -deflection. All steps were repeated until 50 cm (an increase of 10 cm for each subsequent step). The same procedure was applied for other aspect ratios according to the respective value of the z -indicator.

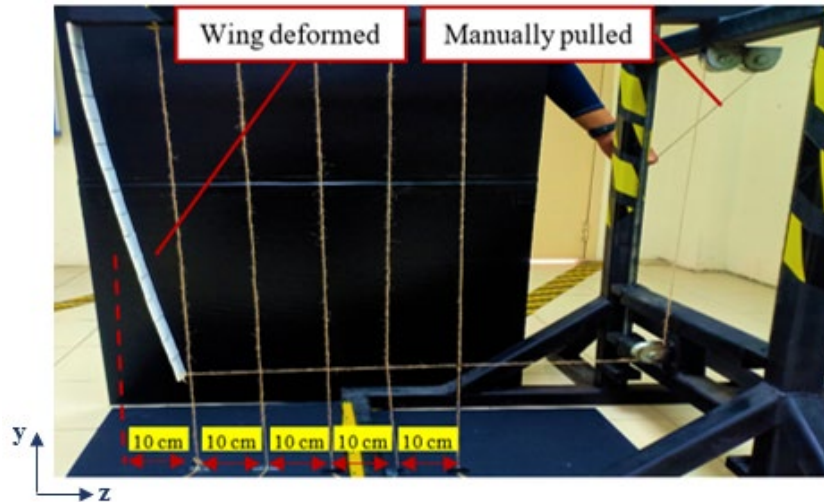
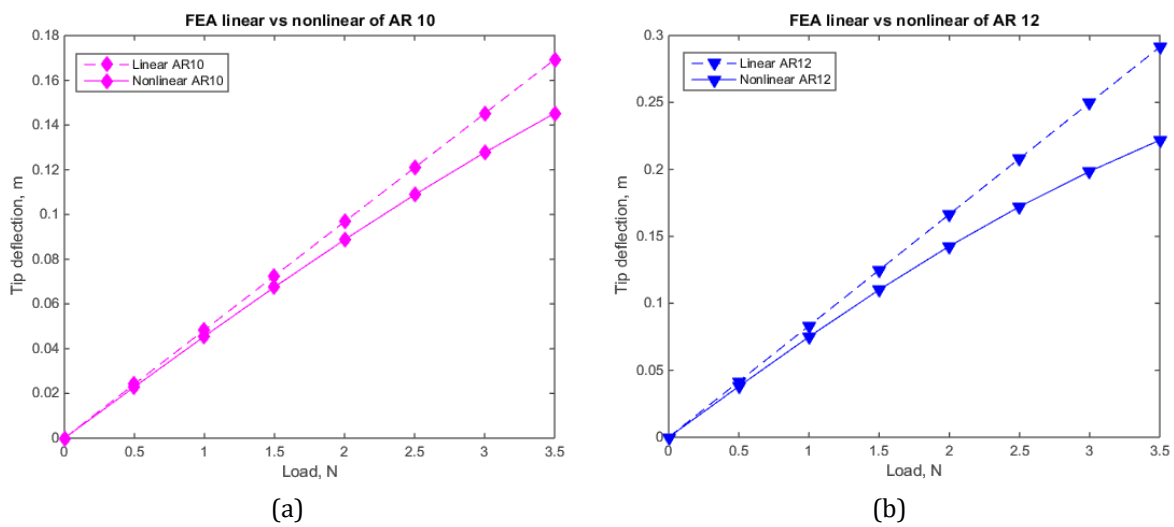


Figure 3. Measurement of y -deflection based on z -indicator

4.0 RESULTS AND DISCUSSIONS

Linear and nonlinear static analyses were considered in this study to examine the influence of geometric nonlinearity for each HAR wing. In particular, the current study compared the deflection of the wing model under various loads. Both linear and nonlinear static analyses were performed using the FE solver of MSC Nastran with the respective solution control code (SOL 101 and SOL 106). The deflection of the wingtip represented the maximum wing deflection. Figure 4 shows the degree of nonlinearity for each model for different aspect ratios under different applied loads (with an increment of 0.5 N at the central node of the wingtip). Referring to Figure 4 (d), the results of the linear static analysis revealed a significant deviation of 44% from the results of nonlinear static analysis for the case of AR-16 under higher loads, as compared to the case of AR-10 (deviation of only 14%).



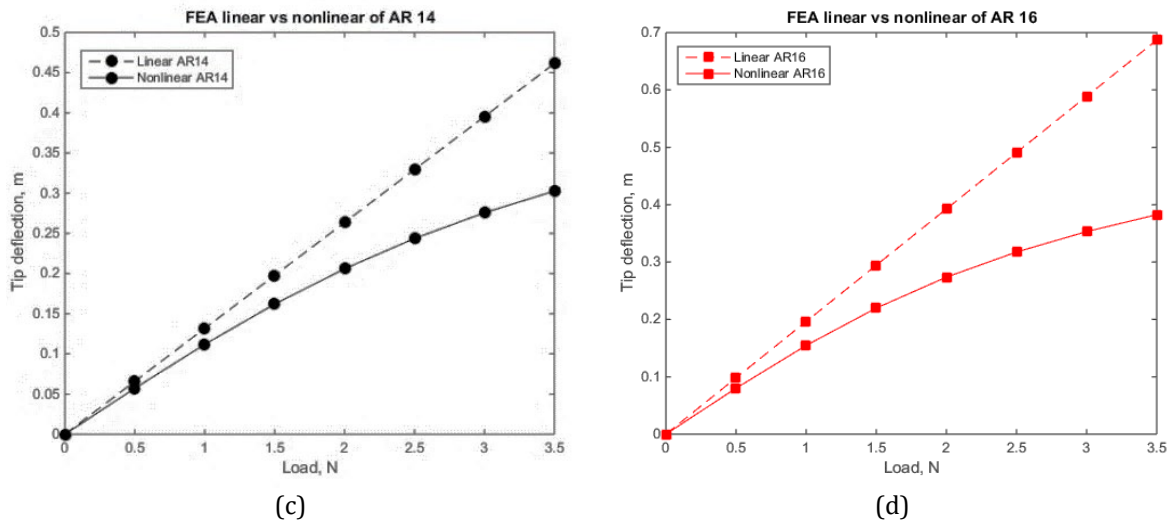


Figure 4. Linear and nonlinear static analyses at (a) AR-10, (b) AR-12, (c) AR-14 and (d) AR-16

The comparison between linear static and nonlinear static analyses results for all aspect ratios are illustrated in Figure 5. The graphs clearly revealed the increase in the wingtip deflection with the increase in wingspan lengths and aspect ratios. Moreover, the difference in the wingtip deflection between linear and nonlinear static analyses was evident. For each AR, the observed deflection in the case of nonlinear static analysis appeared to be substantially lower than the deflection in the case of linear static analysis, which can be attributed to the stiffness hardening effect of the wing model. The effect becomes more visible at the higher magnitude of the deflection of the wingtip. Higher stiffness leads to stiff the wing with higher resistance against the applied force, resulting in lower displacement in the case of nonlinear static analysis. Following the substantial change in wing stiffness, the gap difference between linear and nonlinear static analyses increases with the increase in the wing deflection at a higher load. Furthermore, the linear static analysis may over-estimate the actual bending when large wing deflection is observed. Such attribute adversely influences static and dynamic behaviours, resulting in aeroelastic instability. The linear static analysis can be applied for the case of small wing deflection; the minor change in wing stiffness produces a smaller gap difference between linear and nonlinear static analyses. These findings present valuable insights on the significance of considering geometrical nonlinearity, especially for the application of high aspect ratio wings in actual settings.

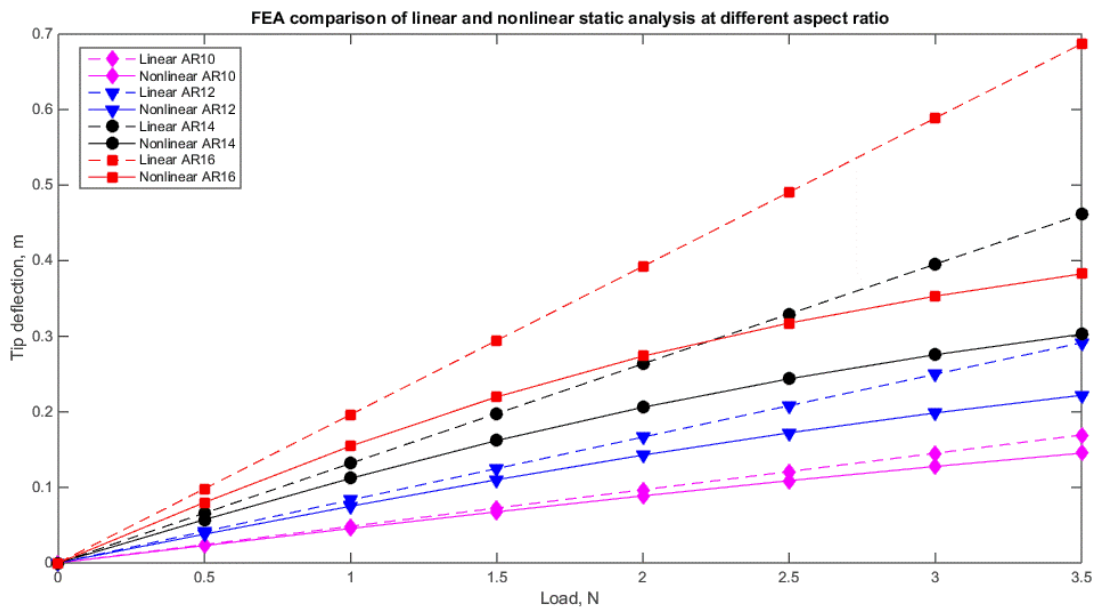


Figure 5. Overall comparison of linear and nonlinear static analyses

The ground static test was performed to verify the conventional FE simulation data, as well as to develop a videogrammetric measurement technique as a preliminary setup prior to the wind tunnel test. The test was conducted by applying concentrated force at the centre chord of the wing tip for each aspect ratio in the undeformed configuration (neglected the gravity effect). The measurement of *y*-deflection via ultrahigh-speed camera for each aspect ratio will be based on the reference of the *z*-indicator (presented in Table 2). The obtained data of *y*-deflection were interpolated based on *z*-indicator to determine the deflection of the wingtip in the *z*-direction.

Table 2. Tip displacement in *y*-direction at different load range

Load, N	<i>Y</i> -deflection, m			
	AR 10	AR 12	AR 14	AR 16
0.5	0.0046	0.0050	0.0046	0.0143
1.0	0.0093	0.0099	0.0139	0.0333
1.5	0.0139	0.0168	0.0286	0.0552
2.0	0.0184	0.0267	0.0447	0.0818
2.5	0.0260	0.0345	0.0606	0.1062
3.0	0.0342	0.0464	0.0713	0.1238
3.5	0.0426	0.0543	0.0909	0.1428

In terms of verification, the results in Figure 6 revealed a similar pattern for all cases of aspect ratios, where the experimental data recorded higher deflection values under the applied loads. For instance, the wing model with an aspect ratio of AR-10 recorded almost similar results for both experimental and simulation cases, with low displacement differences: 0.8 mm at 0.5 N, 1.2 mm at 1.0 N and 1.1 mm at 1.5 N.

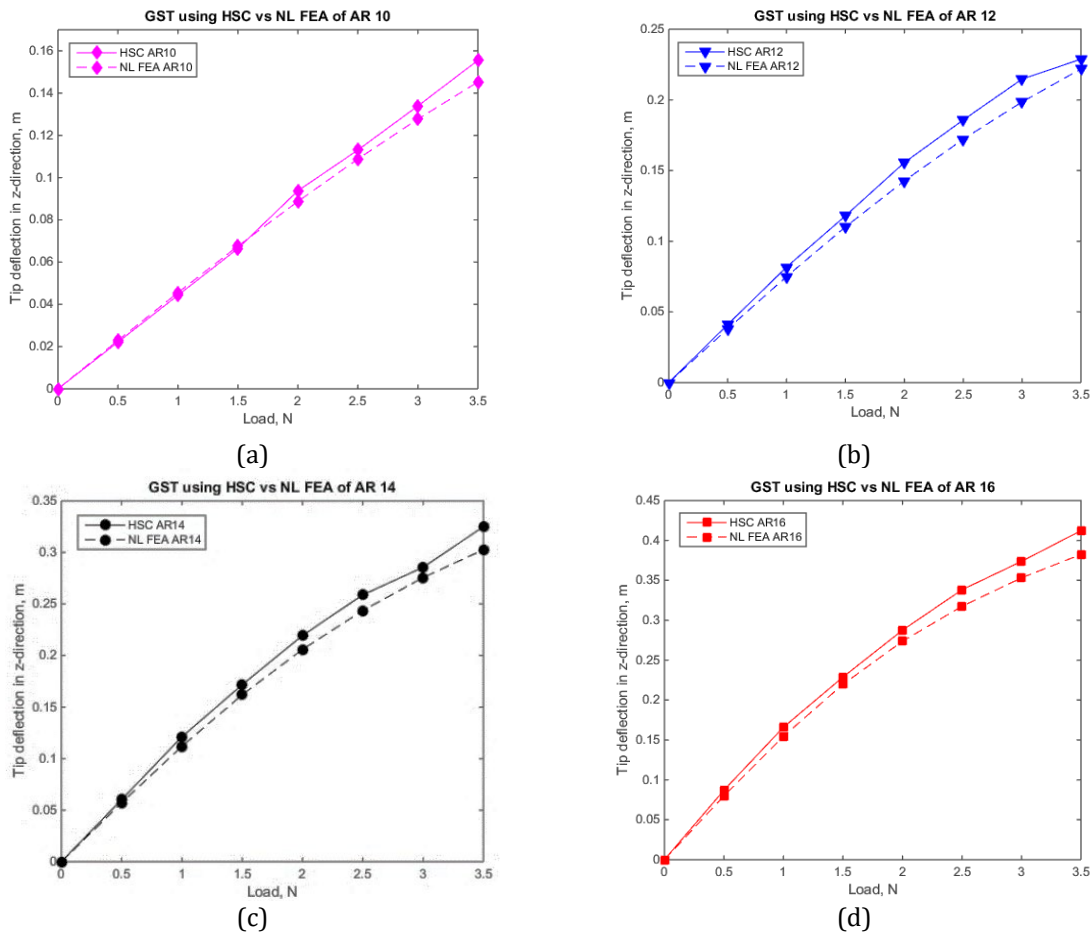


Figure 6. Comparison data between GST using HSC with the conventional FE

However, under the load of 3.5 N, the displacement difference became apparent for the wing model with the same aspect ratio of AR-10, with a percentage difference of 7% which tabulated in Table 3.

Nonetheless, all discrepancies were deemed acceptable, as the recorded percentage difference did not exceed 10%. Figure 7 presents a displacement error for both approaches with the highest error of less than 0.03 m at applied load of 3.5 N. Both cases demonstrated good agreement in terms of the data pattern, where the wingtip deflection increased as the applied load increased. Most of the data on wingtip deflection were higher than the simulation data for all aspect ratios, which may be attributed to human error. The manual release of the applied load substantially influences the deflection of the wing model, and the free-fall condition of the released load exerts additional force to the load due to the gravity force. Therefore, the applied load must be released slowly for higher data accuracy. Another plausible explanation for such deviation involves the effect of the friction between the rope and the grooved wheel of the pulley.

Table 3. Percentage difference between GST and conventional FE

Load, N	Percentage difference in displacement, %			
	AR 10	AR 12	AR 14	AR 16
0.5	3.48	8.05	5.42	8.92
1.0	2.74	8.95	8.28	7.33
1.5	1.67	7.13	6.02	4.14
2.0	5.67	9.09	6.57	5.05
2.5	3.90	7.89	6.25	6.52
3.0	4.88	8.14	3.63	5.84
3.5	7.05	3.13	7.38	7.77

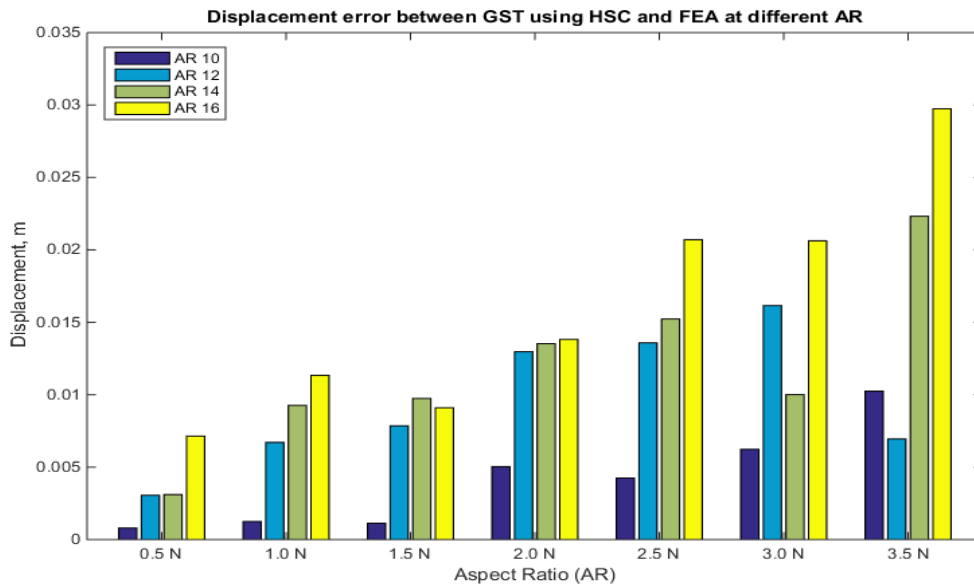


Figure 7. Comparison between GST and conventional FE in displacement error

Besides that, this study identified two key factors from using an ultrahigh-speed camera that may lead to instrumental errors and affect the experimental results. Firstly, an error between the actual value of the image scale size (m/pixel) and the value indicated in the PCC software is possible during the calibration process. Secondly, the motion of the wing deflection under the released load takes place at a significantly high speed, resulting in a poor-quality image taken during the movement. Both factors result in an inaccurate measurement. Capturing the exact value or pixels is only up to a certain precision. The results of the validation in this study demonstrated the appropriateness of identifying z-deflection based on y-deflection using the ultrahigh-speed camera with z-indicator reference for the ensuing wind tunnel test. Evidently, the use of z-indicator reference was deemed novel, as no other prior studies applied such an approach for the case of videogrammetric measurement technique.

5.0 CONCLUSION

With respect to the objectives of this study, the obtained results clearly demonstrated the geometrical effects between linear and nonlinear static analyses for the HAR wing. This study also characterised the nonlinear properties of the HAR wing. Under the same load condition, the physical displacement between

the cases of linear and nonlinear static analyses was significantly different. The deflection is greater at a higher aspect ratio, resulting in a higher deviation for the nonlinear curve, as compared to the linear curve. This can be explained by the constant stiffness for the case of linear static analysis. Unlike the case of linear static analysis, the stiffness for the case of nonlinear static analysis changes (becoming stiffer). In particular, the percentage difference between linear and nonlinear static analyses recorded 44% at aspect ratio of AR-16. The obtained results further reaffirmed the appropriateness of the linear static analysis for the small displacement assumption of the structure. It is essential to consider the nonlinearity effects considering the (high) flexibility of such a structure with large displacement. Furthermore, this study successfully validates the experimental data through the ground static test with simulation data through conventional FE. This study integrated the use of an ultrahigh-speed camera into the videogrammetric measurement technique for the preliminary measurement technique for the case of wing deformation prior to the wind tunnel test. Overall, the experimental and simulation data showed good agreement, with a percentage difference of lower than 10%. This study successfully developed a novel technique that can particularly benefit the future development of the wind tunnel test application.

6.0 ACKNOWLEDGEMENT

The authors acknowledge the financial support for the Ministry of Higher Education, Malaysia and National Defence University of Malaysia (NDUM) for supporting this Fundamental Research Grant Scheme (FRGS) under grant no. FRGS/1/2020/TK0/UPNM/02/9.

List of Reference

- [1] Waitz, I., Townsend, J., Cutcher-Gershenfeld, J., Greitzer, E., & Kerrebrock, J. (2004). Aviation and the environment: A national vision statement, framework for goals and recommended actions.
- [2] Pels, E. (2010). International Air Transport: Environmental Impacts of Increased Activity Levels. *Read Only*, 185.
- [3] Owen, B., Lee, D. S., & Lim, L. (2010). Flying into the future: aviation emissions scenarios to 2050.
- [4] Olsthoorn, X. (2001). Carbon dioxide emissions from international aviation: 1950–2050. *Journal of Air Transport Management*, 7(2), 87-93.
- [5] Nordin, N., Bohari, B., Jemat, M. B., & Harmin, M. Y. (2023). GEOMETRICAL NONLINEARITY OF HIGH ASPECT RATIO WING AND VALIDATION VIA VIDEOGRAMMETRIC MEASUREMENT TECHNIQUE. *Zulfaqar Journal of Defence Science, Engineering & Technology*, 6(2).
- [6] Abbott, I. H., & Von Doenhoff, A. E. (2012). *Theory of wing sections: including a summary of airfoil data*. Courier Corporation.
- [7] McCormick, B. W. (1994). *Aerodynamics, aeronautics, and flight mechanics*. John Wiley & Sons.
- [8] Afonso, F., Leal, G., Vale, J., Oliveira, É., Lau, F., & Suleman, A. (2015, June). Linear vs non-linear aeroelastic analysis of high aspect-ratio wings. In *Congress of Numerical Methods in Engineering* (Vol. 29).
- [9] Harmin, M. Y., & Cooper, J. E. (2011). Aeroelastic behaviour of a wing including geometric nonlinearities. *The Aeronautical Journal*, 115(1174), 767-777.
- [10] Noll, T. E., Brown, J. M., Perez-Davis, M. E., Ishmael, S. D., Tiffany, G. C., & Gaier, M. (2004). Investigation of the Helios prototype aircraft mishap volume I mishap report. Downloaded on, 9, 2004.
- [11] Yagil, L., Raveh, D. E., & Idan, M. (2018). Deformation control of highly flexible aircraft in trimmed flight and gust encounter. *Journal of Aircraft*, 55(2), 829-840.
- [12] Lokos, W., Olney, C., Crawford, N., Stauf, R., & Reichenbach, E. (2002, May). Wing torsional stiffness tests of the active aeroelastic wing F/A-18 airplane. In *43rd AIAA/ASME/ASCE/AHS/ASC Structures, Structural Dynamics, and Materials Conference* (p. 1333).
- [13] Lizotte, A., & Lokos, W. (2005, April). Deflection-based aircraft structural loads estimation with comparison to flight. In *46th AIAA/ASME/ASCE/AHS/ASC Structures, Structural Dynamics and Materials Conference* (p. 2016).
- [14] Northington, J., & Pasilliao, C. (2007). F-16 wing structural deflection testing-phase I. In *2007 US Air Force T&E Days* (p. 1674).
- [15] Gharibi, A., Ovesy, H. R., & Khaki, R. (2016). Development of wing deflection assessment methods through experimental ground tests and finite element analysis. *Thin-Walled Structures*, 108, 215-224.
- [16] Burner, A. W., & Liu, T. (2001). Videogrammetric model deformation measurement technique. *Journal of Aircraft*, 38(4), 745-754.

- [17] Barrows, D. (2007, January). Videogrammetric model deformation measurement technique for wind tunnel applications. In 45th AIAA aerospace sciences meeting and exhibit (p. 1163).
- [18] Black, J. T., Pitcher, N. A., Reeder, M. F., & Maple, R. C. (2010). Videogrammetry dynamics measurements of a lightweight flexible wing in a wind tunnel. *Journal of aircraft*, 47(1), 172-180.
- [19] Zhang, Z. Y., Huang, X. H., Yin, J., & Lai, H. X. (2014). Videogrammetric Techniques for Wind Tunnel Testing and Applications. *Advanced Materials Research*, 986, 1629-1633.
- [20] Nordin, N., Rafi, N. S. M., & Harmin, M. Y. (2020). Nonlinear follower force analysis with ground static test validation of high aspect ratio wing. In *Proceedings of International Conference of Aerospace and Mechanical Engineering 2019: AeroMech 2019*, 20–21 November 2019, Universiti Sains Malaysia, Malaysia (pp. 421-432). Springer Singapore.
- [21] Lähteenmäki, M. (2020). Development and Implementation of Controls for an Optical Spray Chamber.